CCFE-PR(15)29

M. Romanelli, V. Parail, P. da Silva Aresta Belo, G. Corrigan, L. Garzotti,
D. Harting, F. Koechl, E. Militello-Asp, R. Ambrosino, M. Cavinato,
A. Kukushkin, A. Loarte, M. Mattei, R. Sartori

Modelling of Plasma Performance and Transient Density Behaviour in the H-mode Access for ITER Gas Fuelled Scenarios

Modelling of Plasma Performance and Transient Density Behaviour in the H-mode Access for ITER Gas Fuelled Scenarios

M. Romanelli[1], V. Parail[1], P. da Silva Aresta Belo[1], G. Corrigan[1], L. Garzotti[1], D. Harting[1], F. Koechl[2], E. Militello-Asp[1], R. Ambrosino[3], M. Cavinato[5], A. Kukushkin[4], A. Loarte[4], M. Mattei[3], R. Sartori[5]

[1]CCFE, Culham Science Centre, Abingdon, Oxon OX14 3DB, United Kingdom
[2]Technical University Wien, 1020 Vienna, Austria
[3]CREATE, University of Naples "Federico II", Italy
[4]ITER Organization, Route de Vinon-sur-Verdon, CS 90 046, 13067 St. Paul Lez Durance Cedex, France
[5]Fusion For Energy Joint Undertaking, Josep Pla 2, 08019, Barcelona, Spain

The following article appeared in Nuclear Fusion, Vol.55, No.9, September 2015, pp.093008

Modelling of Plasma Performance and Transient Density Behaviour in the H-mode access for ITER Gas Fuelled Scenarios

M. Romanelli[1], V. Parail[1], P. da Silva Aresta Belo[1], G. Corrigan[1], L. Garzotti[1], D Harting[1], F. Koechl[2], E. Militello-Asp[1], R. Ambrosino[3], M. Cavinato[5], A. Kukushkin[4], A. Loarte[4], M. Mattei[3], R Sartori[5]

[1]CCFE, Culham Science Centre, Abingdon, OX14 3DB, UK
[2]Technical University Wien, 1020 Vienna, Austria
[3]CREATE, University of Naples "Federico II", Italy
[4] ITER Organization, Route de Vinon-sur-Verdon, CS 90 046, 13067 St. Paul Lez Durance Cedex, France
[5]Fusion For Energy Joint Undertaking, Josep Pla 2, 08019, Barcelona, Spain

E-mail contact of main author: Michele.Romanelli@ccfe.ac.uk

Abstract. ITER operations require effective fuelling of the core plasma for conditions in which neutral dynamics through the scrape-off layer (SOL) is expected to affect significantly the efficiency of gas penetration. On the basis of previous analysis for stationary conditions, pellets are foreseen to provide core fuelling of high-Q DT scenarios. In this paper we present a modelling study of the gas fuelling efficiency in ITER DT reference scenarios providing an estimate of the upper plasma density achievable with gas fuelling only. Integrated core-edge plasma simulations for various phases of ITER 15 MA/5.3T DT H-mode plasmas, including the stationary H-mode conditions, the H-mode access phase and the preceding L-mode phases, have been carried out with the JINTRAC suite of codes for ITER as well as for lower plasma currents at 5.3T (10 MA, 7.5 MA and 5 MA). In addition a DT plasma scenario with plasma current of 7.5MA and toroidal field of 2.65T representative of lower field operation in ITER has also been studied. The simulations for 15 MA L-mode plasmas indicate that divertor detachment sets the maximum density achievable at the separatrix by deuterium-tritium gas fuelling. This, together with core transport, determines the maximum achievable volume-averaged plasma density, which appears to be ~ 2.5-3.0 10^{19} m^{-3} for a range of SOL transport assumptions considered to be appropriate for these ITER conditions. This level of volume-average density is close to that required for stationary application of NBI heating at full power (16.5 MW per injector) and ion energy (1 MeV) compatible with acceptable shine-through loads on the first wall. For plasma currents of 5-10

MA the maximum achievable L-mode densities with gas puffing are lower than those at 15 MA implying the need for pellet fuelling for L-mode plasmas in ITER to achieve densities in the range of ~ 2.5-3.0 10^{19} m^{-3}. Simulations of gas fuelled DT H-mode plasmas in ITER show that the plasma density increases rapidly after the H-mode transition due to an increased penetration of the neutrals to the core plasma during the initial phase of the H-mode, associated with low divertor power fluxes and the establishment of the edge transport barrier, but that this increase is short lived and saturates as soon as the edge power flux increases and core plasma neutral penetration decreases. The achievable density in gas fuelled H-modes is typically a factor of 2-3 larger than in L-modes for 15 MA DT plasmas in ITER because of the higher edge power flux which raises the detachment limit and the lower plasma collisionalities which increase the anomalous inwards particle pinch. The fusion performance of gas fuelled H-modes at 15 MA is typically found to be moderately high (Q ~ 6-8) due to higher separatrix densities reached and the density in the edge transport barrier being flat (due to low core neutral source), which leads to the pedestal temperature to exceed ~ 6.5 keV and to a high fusion reaction rate throughout the plasma volume. The sensitivity of the modelling results to modelling assumptions and the need for validation of the physics assumptions in the modelling studies are discussed.

1. Introduction

In order to assess the fuelling requirements in stationary L-mode and H-mode operations as well as the plasma behaviour in transients, integrated core-SOL plasma modelling has been carried out for conditions expected in ITER DT scenarios with plasma current 7.5MA and toroidal field 2.65T and plasma currents 15MA, 10MA, 7.5MA, 5MA and toroidal field 5.3T. The latter correspond to time slices during the current ramp-up/down and flat-top operation in the ITER high Q_{DT} baseline scenario while the former is representative of low toroidal field H-mode operation in ITER. The modelling includes: core-particle sources from both gas fuelled neutrals and those recycled at the main-chamber wall and divertor-targets along with their ionization in the SOL, divertor and plasma core and their pumping by the divertor cryo-pumps. The simulations consider all the phases of the H-mode scenarios from the L-mode phase, L-H transition, initial ELM-free H-mode and the stationary H-mode phase with controlled ELMs. The

JINTRAC [1] suite of codes has been used for this analysis. As a first step the edge plasma has been modelled separately for a range of conditions with the EDGE2D/EIRENE code (included in the JINTRAC suite) and previous results obtained with SOLPS have been confirmed [2,3]; namely that, due to the size of the machine, the magnitude of the core plasma neutral source in ITER is typically smaller than 1-2% of the total recycling flux even for conditions far away from semi-detached divertor operation and for plasma temperatures at the divertor in excess of 10 eV [4]. Full plasma simulations have been carried out with JINTRAC in integrated mode with both the Bohm-gyro-Bohm [5] core-transport model and with GLF23 [6] including two impurity species (Be and Ne). The latter species has been introduced in order to evaluate the extrinsic impurity seeding requirements to maintain the peak divertor power flux under 10 MWm^{-2}, which is the ITER divertor design criterion for stationary power fluxes.

2. Simulation setup

For the EDGE2D grid generation the equilibrium map of the 15MA/5.3T ITER reference case has been adopted, with resolution of 65x129 (*see FIG.1(a)*). The poloidal magnetic field is obtained from the derivatives of the Ψ-map. The toroidal magnetic field is represented by $B_{tor}(R)=B_0R_0/R$ where B_0=5.3T and R_0=6.2m. A closed structure to confine the neutral particles has been defined, consisting of the contour of the vacuum vessel and the plasma facing components (*red line, FIG.1(b)*). The divertor dome (*green line, FIG.1(b)*) is also included and the structural support of the dome is represented as semi-transparent surfaces (*blue lines, FIG.1(b)*) with a transparency of 0.5 from both sides. The pump is represented by a pumping surface (*pink line, FIG.1(b)*) between the dome support structures with an albedo of 0.9928. The value of Ψ has been rescaled for the equilibrium at lower currents keeping the shape of the flux surfaces in the SOL. The material for all wall surfaces is assumed to be beryllium and different

surface temperatures are assumed for different wall regions. Thus, the sputtering of tungsten from the divertor is neglected as tungsten transport is not modelled. A grid with a resolution of either 106 rows x 34 rings (for high current H-mode simulations) or 84 rows x 24 rings has been adopted for the simulations with a low level of compression towards the targets, as a compromise between execution time and grid resolution, shown in *FIG.2*. The EIRENE code (coupled to EDGE2D) is used to determine the neutral distribution of all particles, main plasma and impurities, in the SOL. Two impurity species have been included in the simulations: Be as non-recycling intrinsic impurity and Ne as recycling puffed species. In these simulations the main fuel is puffed from the top of the machine consistent with the ITER gas injection geometry with a variable puff rate. Plasma rotation is set to zero at the separatrix and the momentum equation in the core is not solved. The reference simulations are carried out with transport coefficients in the SOL determined by extrapolation from core values to fixed boundary values (at the last SOL surface) which are set-up to $1m^2s^{-1}$ for the heat conductivities and $0.3m^2s^{-1}$ for the diffusivities of main ions and impurities. No SOL particle pinch velocity is included and SOL drifts are not included either. The maximum time step in EDGE2D is 10^{-5}s. For the neutral dynamics, 20000 Monte Carlo particles have been used in EIRENE. A regularly spaced radial grid of 300 points and maximum time step of 10^{-5}s (same as for EDGE2D) have been adopted in JETTO for all simulations in this report. The L-mode simulations have variable ECRH heating while the H-mode simulations are run with variable NBI (power deposition calculated by PENCIL) and ICRH power. For the prediction of anomalous heat, main ion and impurity particle transport in the core, we have adopted the Bohm/gyroBohm (D_{BgB},χ_{BgB}) model in addition to NCLASS for the neoclassical transport. In the case of DT, the transport is calculated separately for each species. However, the difference in transport is expected to be minimal as there is no mass dependence for Bohm diffusion and only a very weak ($\sim m^{1/2}$) dependence for gyroBohm.

Two different sets of coefficients have been adopted for the BgB transport model in the L-mode and in H-mode simulations. In particular, the BgB model used in the H-mode simulations has been determined from the benchmark with GLF23 for the same plasma conditions. The model includes an inwards pinch $v(\rho) = 0.5 \cdot D_{BgB}(\rho) \cdot S(\rho)^2/(dV/d\rho \cdot V(\rho_{sep}))$, where S is the flux surface area and V is the volume enclosed. In the H-mode simulations a fixed-width transport barrier model has been chosen. The barrier width has been fixed to $\Delta\rho_{norm,ETB}$~0.05-6, corresponding to ~6-7 cm at the outer mid-plane. Transport in the barrier region is reduced to approximately ion neoclassical level for all transport channels as a lower limit. ELMs have been modelled with the "Continuous ELM model": when the normalised pressure gradient in the ETB exceeds the imposed alpha critical value, the neoclassical transport is increased in the barrier region gradually in proportion to the difference between the gradient and the critical value [7]. In this manner the normalised ETB pressure gradient is clamped to the value determined by alpha critical, in contrast to the discrete ELM model in which the ETB pressure gradient slowly builds up and then collapses at the onset of an ELM [8]. Radiation is calculated self-consistently from the distribution of impurity ionization states. It should be noted that the radiation due to W is not taken into account, as the transport of W impurities has not been included in these simulations. Nuclear fusion reactions are included as a heat source in all simulations along with sawteeth using either the "Continuous Sawtooth model" (analogous to the continuous ELM model, see above) for the reconnection in the gas flux scans or the Kadomtsev sawtooth reconnection model with user defined minimum sawtooth crash intervals. The transport of He ash is not included.

3. Fuelling in the L-mode phase

Using the JINTRAC settings described in section 2, simulations for the 15MA, 10MA and 5MA L-mode plasmas at 5.3T have been run adopting various levels of ECRH heating and gas fuelling

rates. In this paper we concentrate on the results of the 15MA/5.3T plasmas with 20MW ECRH and varying the rate of D injection from $3.0x10^{21}s^{-1}$ up until divertor detachment is found. Detachment is assumed to be reached when the divertor target temperature gets close to 1eV on an extended region of more than 20 cm from the strike point. The maximum gas rate sustainable (i.e. before detachment) is found to be $1.6x10^{22}s^{-1}$. *FIG. 3* shows the profiles of the neutral source, electron density and electron temperature after simulating 8s of plasma dynamics for three levels of fuelling: $1.0x10^{22}s^{-1}$, $1.3x10^{22}s^{-1}$ and $1.6x10^{22}s^{-1}$. The density profile saturates at a peak density of around $2.9x10^{19}m^{-3}$ (volume average density of ~ 2.2 10^{19} m^{-3}) when the gas puff increases above $1.3x10^{22}s^{-1}$ together with the onset of complete divertor detachment. Hence, higher puff rates do not result in higher core densities than already obtained at this level, but rather only push the plasma closer towards or even into detachment with very small change in density being achieved, which is in line with previous results for the separatrix density in ITER [2,3]. The profiles of the particle source in the SOL-midplane near the separatrix for the three different puff rates is plotted in *FIG. 4* showing the saturation of the neutral source in the SOL for gas fuelling rates larger than 1.3 10^{22} s^{-1}. *FIG. 5* shows the impact of the increased puff-rate on the divertor temperature and power flux and the onset of plasma detachment at the divertor. For the reference choice of the values and radial profiles of the transport coefficient in the SOL for the 15MA scenario, the maximum volume averaged density that can be achieved by gas fuelling is thus below the value compatible with acceptable shine-through loads for stationary application of NBI heating at full power (16.5 MW per injector) and ion energy (1 MeV) in ITER (~2.5-3.0 10^{19} m^{-3}) [9]. For lower values of the plasma current such as 10 MA and 5 MA the maximum achievable density with gas-fuelling only and the reference choice for SOL transport coefficient profiles is typically 1.1 10^{19} m^{-3} for 5 MA and 1.9 10^{19} m^{-3} for 10 MA plasmas with 20 MW of ECRH.

In order to assess the impact of the modelling assumptions on the achievable density for gas fuelling L-modes in ITER we have tested different levels of SOL transport. Results of the simulations performed for 15 MA plasmas (see *FIG. 6.* and *FIG. 7.)* show that the achievable density by gas fuelling depends on the value of transport assumed in the SOL. Thus for values of the particle diffusivity in the SOL under 0.3 m^2s^{-1} and of the thermal conductivity under 1 m^2s^{-1} (similar to levels of effective transport coefficients reported in Alcator C-mod L-mode experiments [10]), it is possible to achieve volume averaged densities above 2.5-3.0x10^{19} m^{-3} compatible with the stationary application of NBI heating at full power and ion energy. This density level taken is thus taken as initial condition for the L-H transition study presented in the next section.

The studies carried out so far indicate that fuelling of L-mode plasmas in ITER to average densities much higher than ~ 3.0 10^{19} m^{-3} with gas fuelling only might not be possible, particularly for lower plasma currents in ITER. Therefore studies are being carried out to study the fuelling of such L-mode plasmas with pellets which is expected to circumvent this limit. In addition, studies on the optimization of the NBI power waveform to access the H-mode in lower current plasmas, so that the plasma density evolution after the H-mode transition (see Sect. 4) ensures acceptable shine-through loads on the first wall panels during this phase, are also in progress.

Obviously, the precise value of the maximum achievable density obtained by gas fuelling in ITER L-modes in the studies presented here depends on modelling assumptions. In this respect a detailed quantitative validation of the integrated modelling approach applied to ITER with experimental results from gas fuelled L-mode density scans in present experiments is required before final conclusions for ITER can be drawn.

4. L-H transition

Modelling of the L-H transition for 15MA/5.3T DT plasmas has been carried out. In the simulations presented in this paper additional heating to a level of 53 MW is applied at 85 s and the H-mode transition is modelled to occur when the loss power exceeds the H-mode power threshold (P_{L-H}) threshold (here the scaling in [11] for the H-mode threshold has been assumed). Following this the transport coefficients in the barrier region are decreased as described in section 3. *FIG. 8* shows the time evolution of a set of selected plasma parameters for a L-H transition in a 15MA/5.3T DT plasma fuelled by gas-fuelling only. Initially, the plasma density increases on a very fast timescale (< 100 ms) due to the change of edge transport after the access to H-mode. The change of edge transport in this phase leads to a reduction of the edge particle/power outflux and to an increased transparency of the edge plasma to neutrals during this phase which causes the fast density rise. However, after this initial phase the plasma density builds up at a much slower rate due to the neutral source and the low value of particle diffusion in the pedestal (close to neoclassical) and finally saturates at values of $\langle n_e \rangle \sim 6.5 \times 10^{19} m^{-3}$(with the onset of ELMs) even for the largest gas-fuelling rates achievable in ITER. Following the L-H transition, the plasma temperature also rises until its value at the pedestal is sufficiently large to exceed the MHD edge stability limit leading to the triggering of ELMs (at the end of the simulations shown in Fig. 8).

5. Gas fuelling in stationary H-mode phases

Simulations of gas fuelled stationary H-mode for a range of currents (5-15MA) at 5.3T and for 7.5 MA/2.65T (representative of low field operation) DT plasmas in ITER has been carried out. The modelled plasmas are heated by both ICRH (20MW) and NBI (33MW) in the simulations of the stationary DT H-mode plasmas along with the intrinsic fusion power. *FIG. 9.-10.* show the

density and electron temperature profiles obtained for 5, 7.5, 10, 15 MA / 5.3 T and 7.5 MA / 2.65 T H-modes by varying the gas puff rate between a minimum level of 0.5-1.0·10^{22} s^{-1} and the applicable maximum without reaching complete divertor detachment. In all cases, core fuelling by neutrals was found to be low (only ~0.5-1.5·10^{21} s^{-1} DT neutral particles penetrate into the core). Due to increased collisionality at the edge, the core plasma inwards particle pinch is only present in the very central plasma region for 5 MA plasmas. The achievable separatrix density by gas fuelling together with peaking of the plasma density due to the core pinch expected in low collisionality plasmas maintain the average density above the acceptable limit for shine-through loads on the first wall (~ 2.5-3.0·10^{19} m^{-3}), which ensures that the full power stationary NBI power of 33 MW and ion energy of 1 MeV used in the simulations can be applied in ITER for these plasma conditions.

At low plasma currents with negligible fusion power, the density tends to saturate as the divertor detachment is approached in a similar fashion to the L-mode simulations. This occurs at larger values of the density than in L-mode simulations because of the increased power flux and lower values of the separatrix transport coefficients in H-mode (cf. gas flux scan at I_p = 7.5 MA / B_0 = 2.65 T in *FIG. 9(b)*). Comparing cases at 7.5 MA, full and half field, the temperature gradient in the core is increased at B_0 = 5.3 T due to reduced sawtooth activity, and the density is higher due to a higher separatrix density for fuelling levels up to 1.0·10^{22} s^{-1}. However, because the SOL heat flux width is larger for 5.3 T than for 2.65 T(due to the longer connection length), this leads to lower SOL power densities and earlier onset of detachment at lower fuelling rates for 5.3 T than for 2.65 T. As a consequence, higher plasma densities are reached at 2.65 T at the highest fuelling rates. For plasma current levels of 10 MA and above the picture of the density behaviour above changes because the fusion power starts to play a role. Already at 10 MA the heat flux through the separatrix is increased by ~20-25 MW due to alpha heating. This allows the

achievement of a higher density at the separatrix by gas fuelling before the onset of detachment, which in turn allows for higher plasma densities in the core to be achievable by gas fuelling. For 15 MA, the plasma density does not saturate at higher gas puff rates, as the fusion power is noticeably increased, amplifying the heat flux crossing the separatrix and thus maintaining the plasma away from detachment. This, together with the presence of an anomalous inward pinch in the core due to the low plasma collisionality plasmas (predicted by GLF23 and correctly reproduced by the retuned BgB model applied here) leads to peaked core density profiles allowing volume average electron density of ~6-7·10^{19} m^{-3} to be reached by gas fuelling only in ITER DT plasmas at 15 MA/5.3T (the density at the separatrix is predicted to range between 5-6·10^{19} m^{-3} in such conditions).

It should be noted that in these simulations the pressure on top of the pedestal is ~120-125 kPa which is in good agreement with estimates from edge MHD stability modelling for ITER [12,13]. Interestingly, for this gas fuelled plasmas the pressure increase in the pedestal zone is due almost exclusively to the large temperature gradients in the ETB, as the density profiles in the ETB are almost flat. This is the consequence of negligible neutral penetration across the separatrix into the core plasma and the lack of a pinch in the barrier region (assumed in this modelling). Modelling results for ITER show that for a gas fuelling level of 3.0·10^{22} s^{-1}, Q ~ 7.5 can be achieved, even if the core fuelling by neutrals remains at the low level of ~10^{21} D+T particles (*see FIG. 10(b)*). This high fusion performance without core fuelling by pellets is obtained in the simulations because it is assumed that the maximum achievable separatrix density by gas fuelling is only determined by the detachment limit in ITER H-modes and that increasing gas fuelling has no influence on the maximum pressure that can be achieved in the H-mode pedestal. Present experiments in H-mode plasmas show that increasing plasma density

by gas fuelling tends to decrease the pedestal pressure and overall energy confinement in H-mode, which can be due to the increased plasma collisionality affecting the edge current magnitude and thus edge MHD stability, to the increased neutral penetration increasing transport in the pedestal barrier, etc. It is presently unknown if such behaviour will be found in ITER or not, as some of the physics mechanisms invoked to explain present experimental results (i.e. decreased edge current density due to high collisionality or large core plasma neutral source) are not expected to play a significant role in ITER.

In addition, it is possible that the small outflux from the core plasma for these gas fuelled H-modes may not produce the required helium exhaust to maintain the helium density at a level of ~ 5% compatible with stationary high Q_{DT} plasmas in ITER. For an alpha heating power of 100 MW the stationary helium core plasma production and stationary helium exhaust required is 1.8 10^{20} s^{-1}, which corresponds to a minimum DT outflux of 3.6 10^{21} s^{-1} for 5% helium concentration assuming similar particle transport for DT and He. This value is already larger than the maximum core neutral source obtained in these simulations and would further increase due to the expected helium de-enrichment at the divertor which increases the pumped DT throughput and associated core plasma outflux to achieve a given net helium ash removal rate from the core plasma. Further modelling studies including helium transport and exhaust are under progress to assess the fusion performance achievable in these gas fuelled H-modes and the duration over which it can be eventually sustained in ITER.

It is also important to note that these optimistic results for the core density and Q achievable in ITER 15 MA plasmas with gas puffing also rely on the presence of an anomalous pinch in the core, and, even more importantly, on assumptions of the reduction of anomalous transport in the

SOL in H-mode plasmas. In these simulations it is assumed that the reduction of anomalous transport observed in the edge transport barrier slightly extends into the SOL. This is observed in present-day experiments and is the physics mechanism invoked to explain the observed scaling of the scrape-off layer power width in H-modes in present experiments [14]. Without extension of at least a few millimetres of the low transport domain of the ETB beyond the separatrix, the heat flux would spread over a wider area on the target plates, due to increased perpendicular transport, and detachment would be reached at much lower gas flux rates. The precise choice for the reduction of transport in the SOL of H-mode plasmas and the level of impurities at the divertor, which contribute to radiated power losses and to the decrease of divertor temperature affecting detachment onset, lead to a much higher level for the separatrix densities to be achievable in our simulations compared to original ITER studies [15]. These were performed with larger anomalous transport coefficients (uniform in the SOL) [15] and carbon impurities. More recent studies carried out with transport coefficients similar to those in the integrated modelling presented here show similar values for the saturation of the separatrix density in ITER to those reported here [16] (see Section 6 for a more detailed discussion of this issue).

The achievable separatrix density before the onset of detachment is also influenced by the presence of W (not considered in these studies) and the puffing of Ne because of the associated increase of plasma radiative losses in the core and SOL divertor. It should be noted that large radiative losses are expected to be required in ITER for high Q_{DT} plasmas to maintain the peak divertor heat load below 10 MW m^{-2}. According to estimates for the power density reaching the inner and outer target (*see FIG. 11.*) to reduce the peak divertor heat load under this limit requires gas fuelling levels equal or higher than $3 \cdot 10^{22}$ s^{-1} for the Ne seeding levels explored in

this study which lead to core Ne concentrations of typically only 0.05 %. These gas fuelling levels correspond to a separatrix density equal or higher than 6.0 10^{19} m^{-3}, as shown in Fig. 10.a.

A summary of the plasma parameters in ITER 5.3T H-modes for currents of 5, 7.5, 10 and 15 MA at the highest density achieved by gas fuelling only with the integrated modelling tools and assumptions described above is shown in *FIG. 12.*

As in the case of L-mode simulations, a detailed quantitative validation of the integrated modelling approach applied to ITER with experimental results from gas fuelled H-mode density scans in present experiments is required before final conclusions for ITER can be drawn. In the case of H-mode conditions this requires not only the validation of the SOL modelling assumptions setting the maximum achievable separatrix density but also of the MHD stability and transport assumptions in the ETB for H-mode plasmas with high plasma density, low pedestal collisionality and low neutral source in the pedestal region. Such validation requires dedicated experiments at the highest currents and powers achievable in the existing tokamaks to approach these ITER-like conditions.

6. Impact of ETB/SOL transport on gas fuelling of ITER stationary H-modes

Scans in ETB and SOL transport assumptions have been performed for the 15 MA / 5.3 T gas fuelled H-mode scenario at low core impurity concentration (Z_{eff} ~ 1.02-1.10) (i.e. low Ne seeding) to assess the sensitivity of the predicted achievable core density, fusion performance and resulting divertor target power loads on uncertainties in edge transport conditions. In one scan, the width of the extension of the reduced transport zone (or ETB extension) into the SOL was kept fixed at $\Delta_{ETB\rightarrow SOL}$ ~5-6 mm (at the outer midplane) and the ETB width itself was varied in a range between $\Delta_{ETB,\rho tor,norm}$ = 0.05-0.09, corresponding to 5-10 cm at the outer midplane.

This was done while adjusting the critical pressure gradient in the ETB so that the pressure on top of the pedestal was maintained at a level p_{ped} ~ 120-130 kPa for all conditions. To ensure a fast convergence to stationary conditions a low gas flux rate of $\Gamma_{DT} = 10^{22}$ s^{-1} was prescribed for this scan. Another scan was performed with fixed $\Delta_{ETB,ptor,norm} = 0.07$, corresponding to ~7-8 cm at the outer midplane, and without any extension of the reduced transport into the SOL (similar to transport assumptions in previous ITER studies [15, 17]). For this second scan the gas flux rate has been varied within $\Gamma_{DT} = 1\text{-}3\cdot10^{22}$ s^{-1}.

The results of these two scans are shown in *FIG. 13* and a summary of selected plasma parameters for these simulations are summarized in *TABLE 1*. The results for scan 1 demonstrate that uncertainties for the level of transport in the ETB and in its extension into the SOL or uncertainties for the width of the ETB itself lead to a comparably low variations in the predicted core density of Δn_e ~ $1.0\text{-}1.5\cdot10^{19}/m^3$ for low gas fuelling rates. A reduction in the ETB width at constant pedestal pressure and at constant heat flux from the core yields a reduction in heat conductivities in that zone, associated with the appearance of larger gradients in temperature. These steeper gradients are also present in the SOL region where the ETB transport is applied leading to a reduction of the power decay length λ_q and to a higher separatrix density for the same gas fuelling rate. This effect is expected to be more pronounced at increased gas flux rates where larger variation in separatrix densities should be obtained due to the varying detachment limit with λ_q consistent with previous edge modelling studies for ITER [16]. It should be noted that in these simulations the impurity content is extremely low (trace amounts of Ne, core Be concentration of < 0.5% and W not considered), which leads to an improved plasma performance compared to the simulations in Section 5 due to reduced dilution and radiation in the core (Q_{fus} ~ 7-8 is predicted already for $\Gamma_{DT} = 10^{22}$ s^{-1}). The low level of impurities together with the low gas

fuelling rates leads to peak divertor power loads of ~ 20 MW/m^2, which are a factor of 2 larger than the stationary power handling limit of the ITER W divertor. In this scan, the transport in the far SOL (i.e. beyond the region of reduced anomalous transport due to the H-mode) has not been varied. However, the dependence of the predicted core density on $\chi_{far\ SOL}$ and $D_{far\ SOL}$ is expected to be smaller compared to the L-mode results, because the core plasma properties are mainly determined by transport assumptions in the ETB and the vicinity of the separatrix, which in these H-mode simulations are determined by the choice of transport in the ETB.

Scan 2 provides an estimate for the uncertainty in plasma core density and performance predictions due to the unknown size of the ETB width extension into the SOL, and it provides an opportunity to do a closer comparison with predictions for similar ITER plasma configurations that have previously been studied by combined simulations of B2-EIRENE and ASTRA [15,17] with the same SOL transport assumptions (constant $\chi_{i,e}$ = 1.0 m^2/s and D_i = 0.3 m^2/s throughout the SOL plasma without any reduction near the separatrix due to extension of the ETB extension in the SOL). Comparing simulation cases at low gas flux rate $\Gamma_{DT} = 10^{22}$/s with and without the ~5-6 mm extension of the ETB into the SOL (Cases 2 vs. Case 4), the core density and fusion power are slightly reduced ($\Delta n_e \sim -0.5 \cdot 10^{19}$/m^3, $\Delta P_{fus} \sim$ -20 MW) for the case without the ETB extension. These changes are caused by an increase in λ_q due to the increase of the transport coefficients from the values typical in the ETB to the larger and constant value in the SOL for Case 4 compared to Case 2. This variation in the achieved separatrix density for a given gas flux related to the specifications of the near-separatrix SOL transport is expected to be larger at larger fuelling rates as detachment is strongly influenced by λ_q, in agreement with previous edge plasma simulation studies for ITER [16]. Comparing Cases 4-6 with similar conditions in [15] (P_{AUX} = 53 MW, $\langle n_{D+T} \rangle \sim 6\text{-}8 \cdot 10^{19}$/m^3), the predictions for core fusion performance and for the

power crossing the separatrix are found to be similar between the two modelling approaches (e.g. $Q_{fus} \sim 7$ vs. $Q_{fus} \sim 5\text{-}6$ and $P_{SOL} \sim 120$ MW vs. $P_{SOL} \sim 110$ MW for Case 4 with respect to similar conditions in [15]). Indeed more recent simulations with ASTRA including the self-consistent evaluation of the pedestal pressure from the EPED1 model and the SOL relations derived from B2-Eirene in [15] find similar values of Q_{fus} for the densities modelled with the JINTRAC suite [18]. In addition, the SOL parameter relation for the maximum power density at the target plates (including power deposited by radiation and neutral interaction) given in equations (1) and (4) in [15] seems to apply quite well also to the Cases 4-6 considered here. The neutral influx at the separatrix has the same order of magnitude as that predicted by equation (5) in [15] ($\Gamma_{D,T,neut,sep} \sim 10^{21}$/s). The relative dependency of μ (related to the degree of detachment of the divertor) with respect to the main ion separatrix density can be expressed for Cases 4-6 as $n_{D+T,sep} \propto \mu^{C}$, $C \sim 0.4\text{-}0.5$ and thus seems to fit well with the scaling $n_{D+T,sep} \propto \mu^{0.43}$ given in [17].

However, in absolute terms, the predicted main ion density at the separatrix is significantly higher in Cases 4-6 than that given by equation (8) in [15]. According to equation (8), $n_{D+T,sep} \sim 4 \cdot 10^{19}/m^3$ for $P_{SOL} \sim 120$ MW, whereas $n_{D+T,sep} \sim 4.5\text{-}6.5 \cdot 10^{19}/m^3$ for Cases 4-6, although the normalised neutral pressure is still rather small at the applied gas flux rates $\Gamma_{DT} \leq 3 \cdot 10^{22}$/s, $\mu < \sim 0.70$, which means that the saturation level for the separatrix density could be even higher. It should be noted that from the point of view of divertor power load control, only Case 6 is marginally compatible with the requirement of maintaining the peak divertor heat flux under 10 MWm^{-2}. Because of the discrepancy in $n_{D+T,sep}$ in absolute terms, the same fusion performance can be obtained in the JINTRAC calculations at much lower particle source rates and μ with gas fuelling only, whereas in [15] some pellet fuelling had to be considered to achieve high core densities at limited $n_{D+T,sep}$. These differences in separatrix densities are related

to the impurity species and levels considered in the two simulations levels (JINTRAC: Be, Ne, B2-EIRENE/ASTRA: He, Be, C) with, probably, a smaller influence of the assumptions for the material of plasma facing components (JINTRAC: Be+W, B2-EIRENE/ASTRA: C). In fact the impurity concentration in Cases 4-6 (Z_{eff} < 1.1) is significantly lower compared to the simulations in [15] in which significant C sputtering is present and Z_{eff} > ~1.7 at the separatrix for P_{SOL} ~ 120 MW according to equations (6), (8) and (11) in [15]. The increased impurity content leads to an increase of the radiation in the SOL by ~30-40 MW in the simulations in [15] compared to Cases 4-6, which leads to lower separatrix densities in the B2-Eirene/ASTRA studies. Indeed, as already mentioned in [17] and in previous ITER edge modelling studies, simulations with low impurity content of ITER high Q_{fus} scenarios would require very high separatrix densities to achieve divertor power load control. These were considered not to be compatible with high pedestal pressure/high energy confinement required for high Q_{fus} in ITER on the assumption that the plasma behaviour observed in present experiments can be extrapolated to ITER, which as mentioned above remains to be proven.

Indeed, simulations with JINTRAC with Be divertor targets and low gas flux of $\Gamma_{DT} = 0.75 \cdot 10^{22}$/s (not shown here) have a higher Zeff ~ 1.7-1.8, increased impurity radiation in the divertor and SOL and degraded fusion performance with P_{SOL} ~ 95 MW. For such simulations, the main ion density at the separatrix dropped down to lower values $n_{D+T,sep}$ ~ $2.5 \cdot 10^{19}/m^3$ similar to those obtained for comparable conditions in [15]. Taking into account the discrepancies in impurity modelling assumptions, good overall agreement has thus been found between independently performed JINTRAC and B2-EIRENE/ASTRA predictions for the

15 MA ITER baseline scenario core and edge plasmas, which strongly supports the validity of both of these integrated modelling approaches for stationary conditions.

6. Conclusion

Simulations of gas fuelled plasmas have been carried out with the JINTRAC suite of codes for ITER plasmas at 15 MA, 10 MA, 7.5 MA and 5 MA / 5.3 T and 7.5MA / 2.65 T. The simulations at 15 MA indicate that, for a range of transport assumptions compatible with observations in present tokamaks, the maximum achievable density with deuterium-tritium gas fuelling only is in the range of 2.2 and 3.5 $x10^{19}$ m^{-3} in the L-mode phase, limited by the onset of divertor detachment. These density values are similar to those required for stationary application of the NBI at full power and ion injection energy in ITER with acceptable shine-through loads on the first wall, particularly taking into account the modelled density evolution after the H-mode transition. For lower plasma currents the achievable plasma densities by gas fuelling in the modelled L-mode plasmas are lower than those for 15 MA. While the accuracy of these predictions for ITER requires detailed validation of the models applied with present experimental results from L-mode gas fuelled density scans, the studies carried out so far indicate that pellet injection may have to be applied more routinely to fuelling of L-mode plasmas in ITER, particularly for lower plasma current levels, than originally foreseen. Studies are in progress to model pellet fuelling of these ITER L-mode plasmas with the same tools as in the present study.

Modelling of the H-mode transition, following the increase of additional heating beyond the L-H threshold power, shows that the pedestal density can be increased to a level of 5-6$x10^{19}$ m^{-3} by gas fuelling only in ITER for a plasma current of 15 MA. This density level can be maintained

during the whole stationary H-mode phase with a puffing rate of 2-3x10^{22} s^{-1} or even further increased once a significant amount of fusion power is generated.

The Q obtained with gas-puff only for gas fuelled 15 MA/5.3T plasmas in ITER is found to reach about Q ~ 7-8. It should be noted that the sustainment of such high Q conditions over long timescales with gas fuelling is questionable due He ash accumulation in the core plasma and further modelling studies are in progress to assess this issue quantitatively. The present studies are thus in agreement with previous ITER evaluations which indicated the need of pellet fuelling for the achievement of the high density required for the Q = 10 baseline scenario in ITER and to provide the required helium exhaust to maintain it over long timescales. The modelled fusion performance of the 15 MA gas fuelled ITER H-mode plasmas in our studies depends critically on two assumptions:

a) that the achievable separatrix density in high energy confinement H-modes is solely limited by divertor detachment, which allows the increase of the separatrix density by gas puffing up to the level in which strong divertor detachment sets in and divertor peak power fluxes decrease under 10 MWm^{-2} with minimum contribution of impurity radiation in the SOL/divertor; and

b) that the existence of flat density profiles in the ETB (associated with the low neutral source for these gas fuelled plasmas) will not alter the reduction of the transport in this region associated with H-mode confinement nor the edge plasma MHD stability, thus allowing pressures up to the edge MHD limit expected for the low collisionality ITER pedestal plasmas to reached.

Both of these modelling assumptions require confirmation from dedicated experiments and comparison with the integrated modelling tools applied to model ITER in order to strengthen the basis for the results presented in this paper.

Acknowledgments

This work was funded jointly by the RCUK Energy Programme [grant number EP/I501045] and ITER Task Agreement C19TD51FE (implemented by Fusion for Energy under Grant GRT-502). The views and opinions expressed do not necessarily reflect those of Fusion for Energy which is not liable for any use that may be made of the information contained herein. The views and opinions expressed herein do not necessarily reflect those of the ITER Organization.

REFERENCES

[1] ROMANELLI, M., *et al*. Plasma and Fusion Research **9** (2014) 3403023.

[2] KUKUSHKIN, A.S., et al., Nucl. Fusion **53** (2013) 123024.

[3] KUKUSHKIN, A.S., et al., Nucl. Fusion **53** (2013) 123025.

[4] LOARTE, A., et al., to be published in J. Nucl. Mat. 2015.

[5] ERBA, M., et al., Pl. Phys. Control. Fusion **39** (1997) 261.

[6] WALTZ, R. E., et al*.,* Phys. Plasmas **4** (1997) 2482.

[7] PARAIL, V., et al., Nucl. Fusion **49** (2009) 075030.

[8] WIESEN, S., et al., Plasma Phys. Control. Fusion **53** (2011) 124039.

[9] OIKAWA, T., et al, Proc. 31st Japanese Physical Society Meeting, Niigata, Japan, 2014.

[10] LABOMBARD, B., et al., Phys. Plasmas **8**(2001) 2107.

[11] MARTIN, Y. R., et al., J. Phys.: Conf. Ser. **123**(2008) 012033.

[12] SNYDER, P. B., et al., Nucl. Fusion **51** (2011) 103016.

[13] MAGET, P., et al., Nucl. Fusion **53** (2013) 093011.

[14] EICH, T., et al., Nucl. Fusion **53** (2013) 093031.

[15] PACHER, H. D., et al., Journal of Nuclear Materials **415** (2011) S492.

[16] KUKUSHKIN, A. S., et al., J. Nuc. Mat. **438** (2013) S203–S207.

[17] PACHER, G. W., et al., Nucl. Fusion **48** (2008) 105003

[18] POLEVOI, A. et al., Proc. 25th IAEA Fusion Energy Conference, St. Petersburg, Russia, 2014, paper PPC/P3-2, submitted to Nucl. Fusion.

FIGURES

Fig. 1 (a)

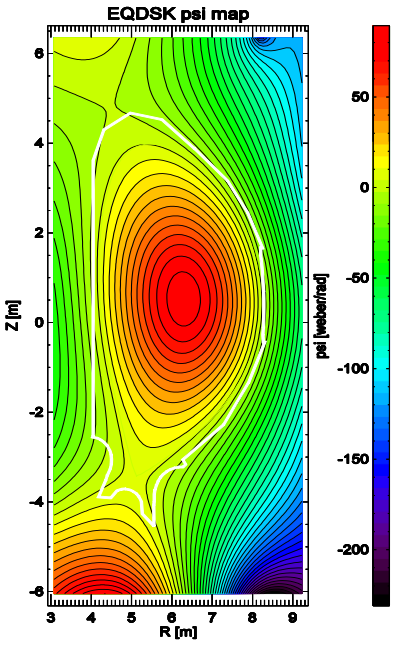

Fig. 1(b)

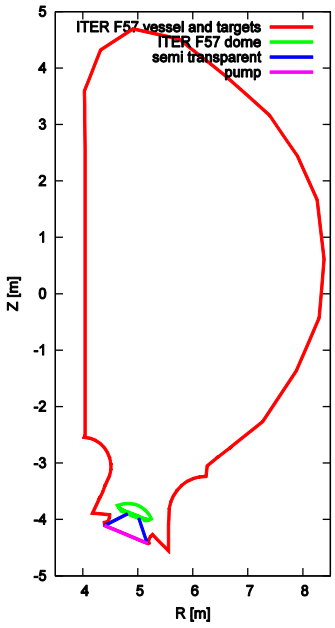

FIG. 2

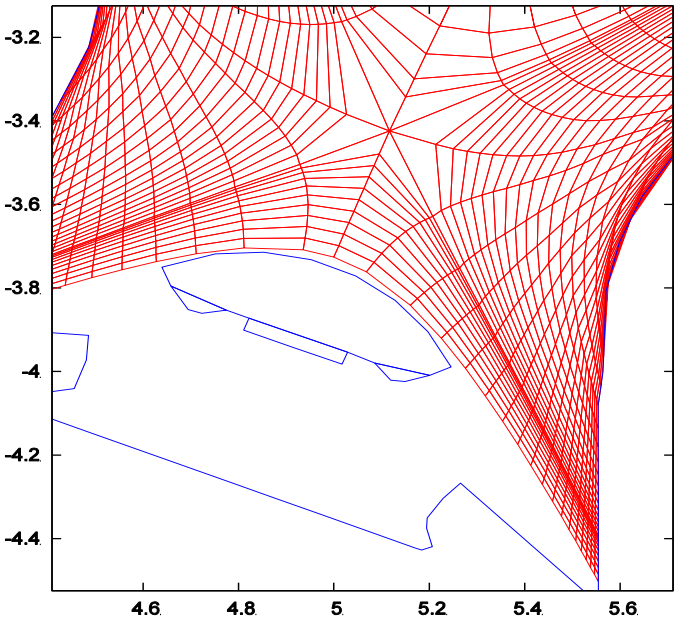

FIG. 3(a)

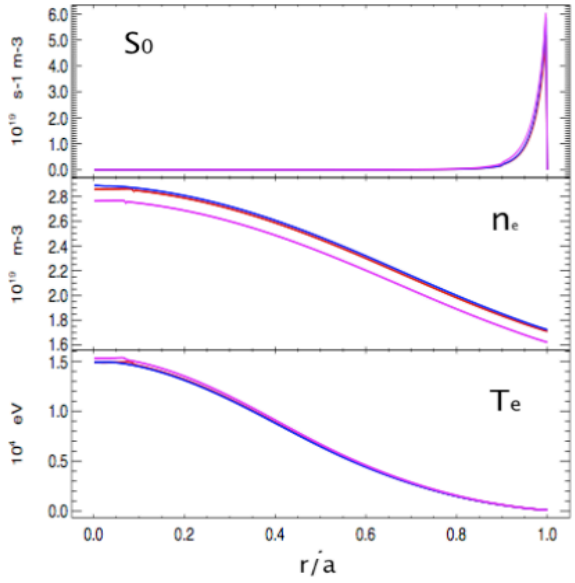

FIG. 3(b)

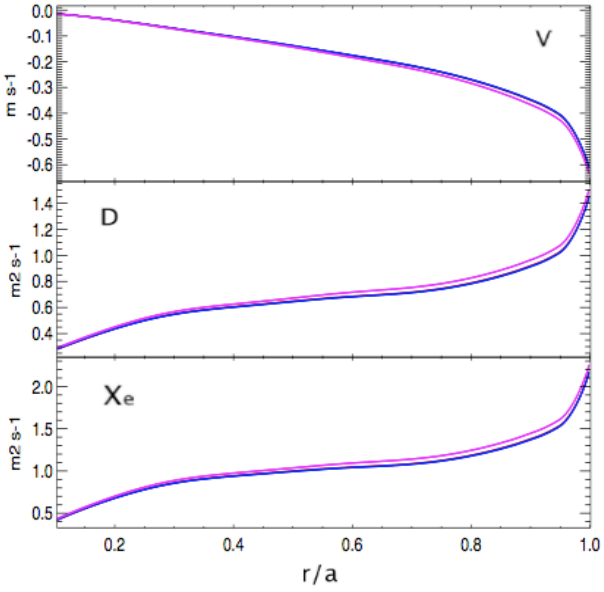

S_0

FIG. 4

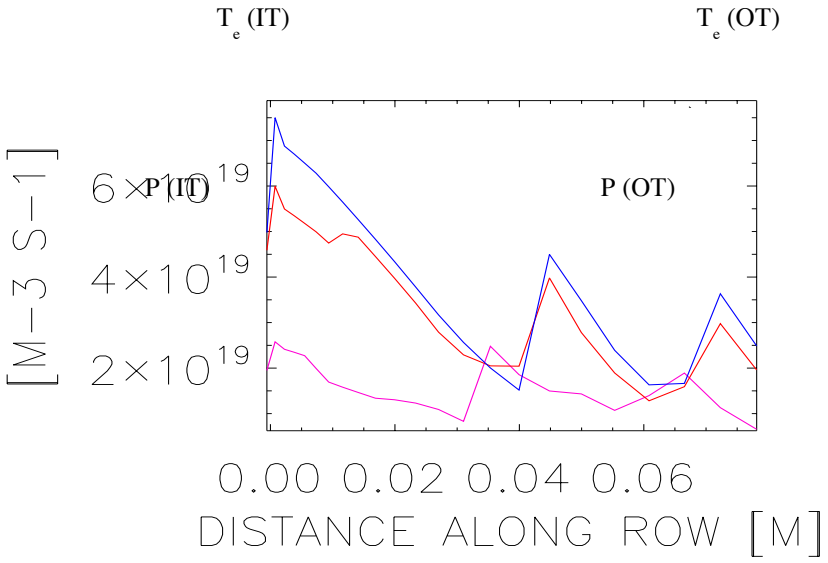
T_e (IT)
T_e (OT)
P (IT)
P (OT)
[M−3 S−1]
6×10^19
4×10^19
2×10^19
0.00 0.02 0.04 0.06
DISTANCE ALONG ROW [M]

FIG. 5

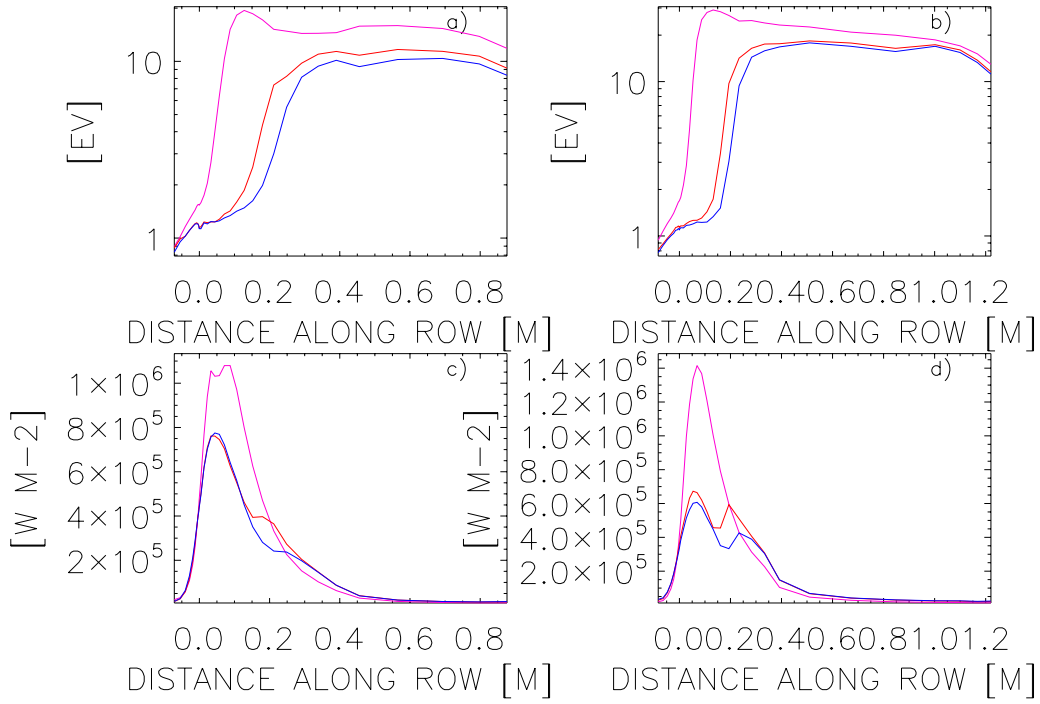
a)
b)
c)
d)
[EV]
10
1
0.0 0.2 0.4 0.6 0.8
0.00.20.40.60.81.01.2
DISTANCE ALONG ROW [M]
[W M−2]
1×10^6
8×10^5
6×10^5
4×10^5
2×10^5
1.4×10^6
1.2×10^6
1.0×10^6
8.0×10^5
6.0×10^5
4.0×10^5
2.0×10^5

χ_i χ_e

FIG. 6

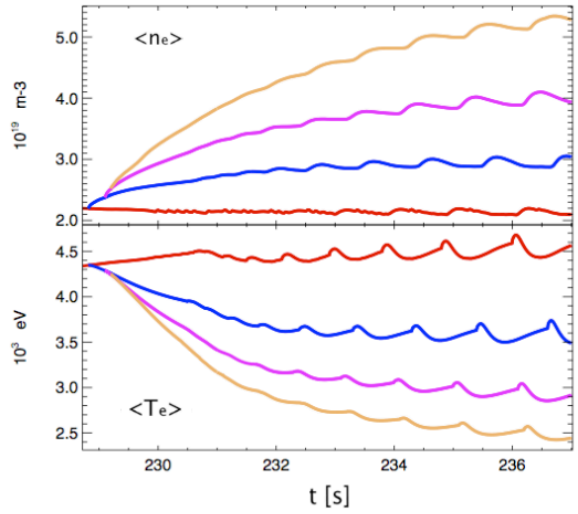

FIG. 7

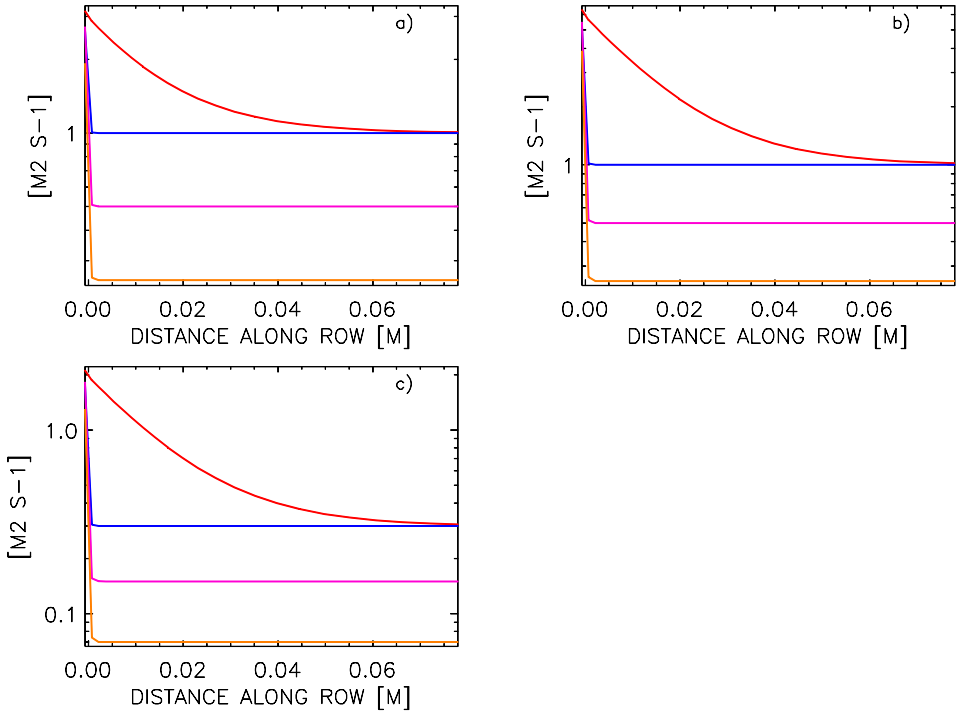

FIG. 8(a)

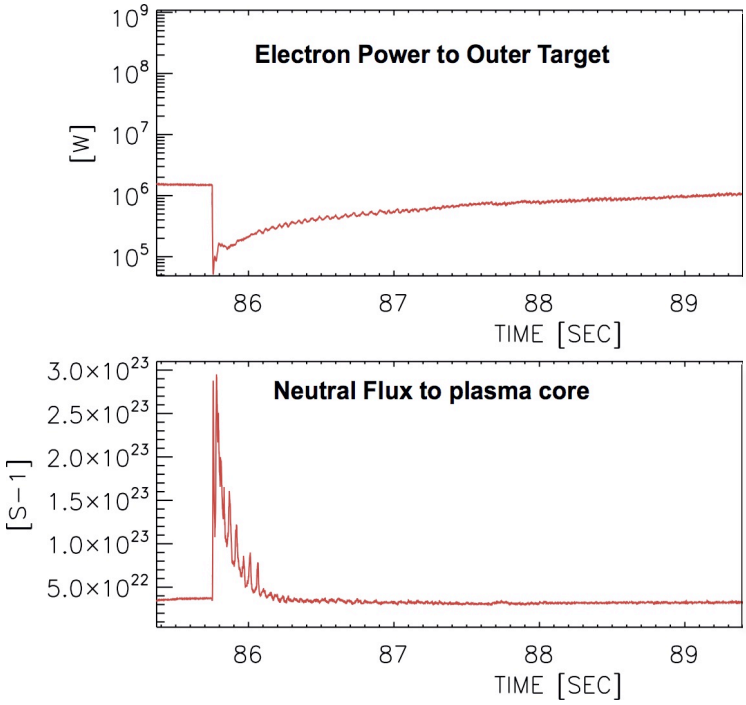
Electron Power to Outer Target
[W]
10^9
10^8
10^7
10^6
10^5
86
87
88
89
TIME [SEC]
Neutral Flux to plasma core
[S-1]
3.0×10^{23}
2.5×10^{23}
2.0×10^{23}
1.5×10^{23}
1.0×10^{23}
5.0×10^{22}
86
87
88
89
TIME [SEC]

FIG. 8(b)

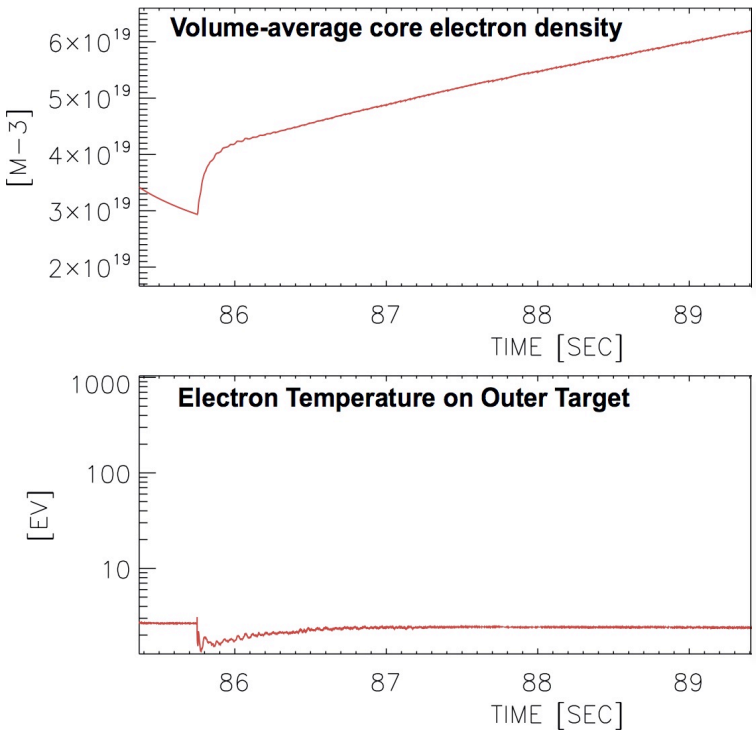
Volume-average core electron density
[M-3]
6×10^{19}
5×10^{19}
4×10^{19}
3×10^{19}
2×10^{19}
86
87
88
89
TIME [SEC]
Electron Temperature on Outer Target
[EV]
1000
100
10
86
87
88
89
TIME [SEC]

n_e
n_e

FIG. 9(a)

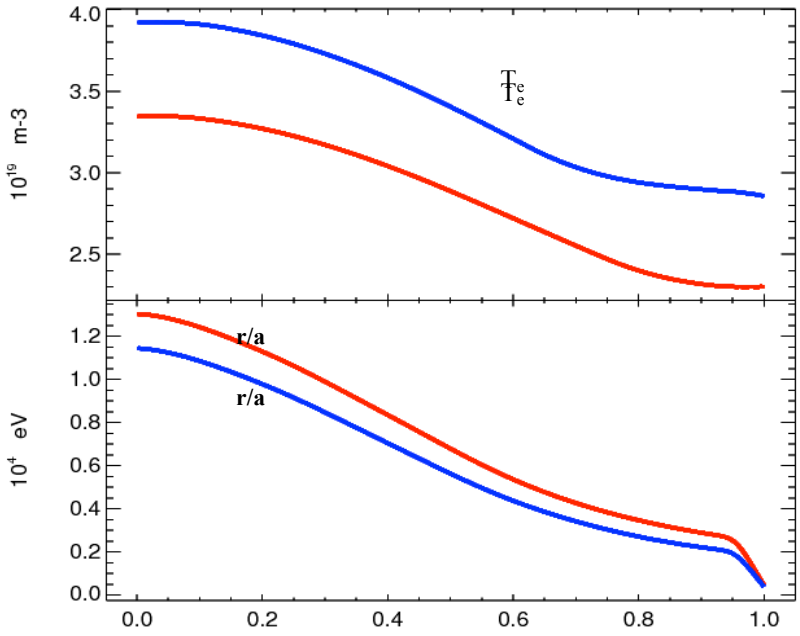

FIG. 9(b)

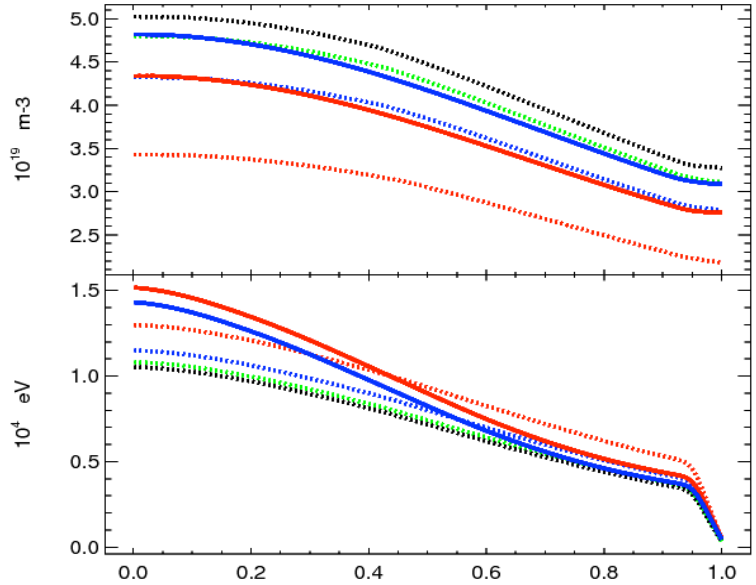

n_e
n_e

FIG. 9(c)

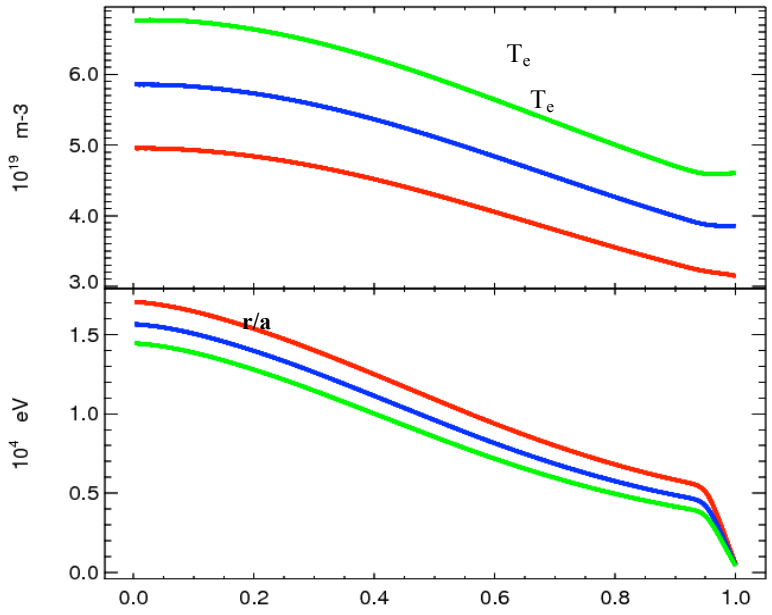

FIG. 10(a)

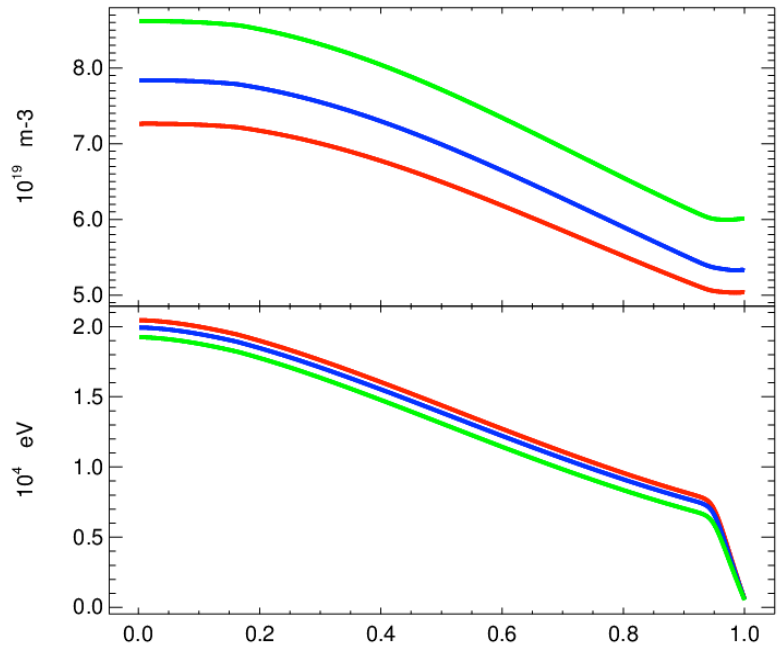

P_{in}

Q

FIG. 10(b)

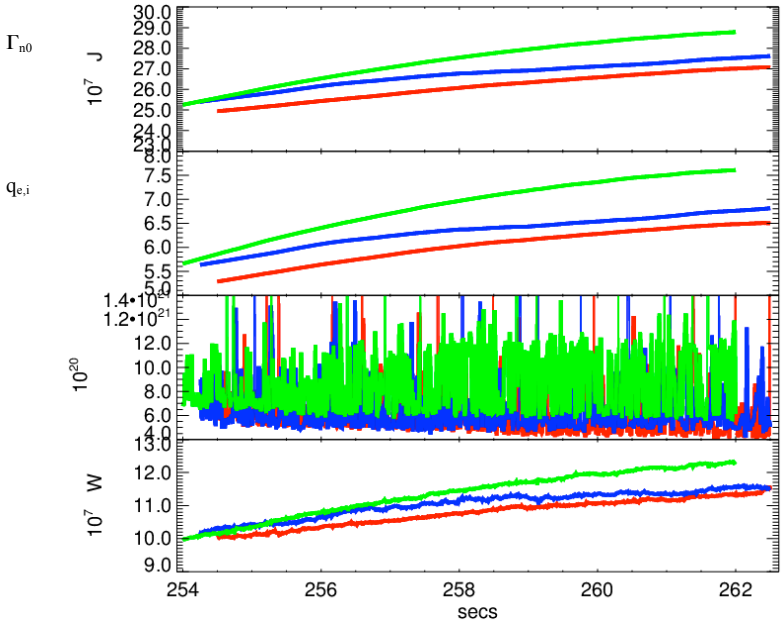

FIG. 11(a)

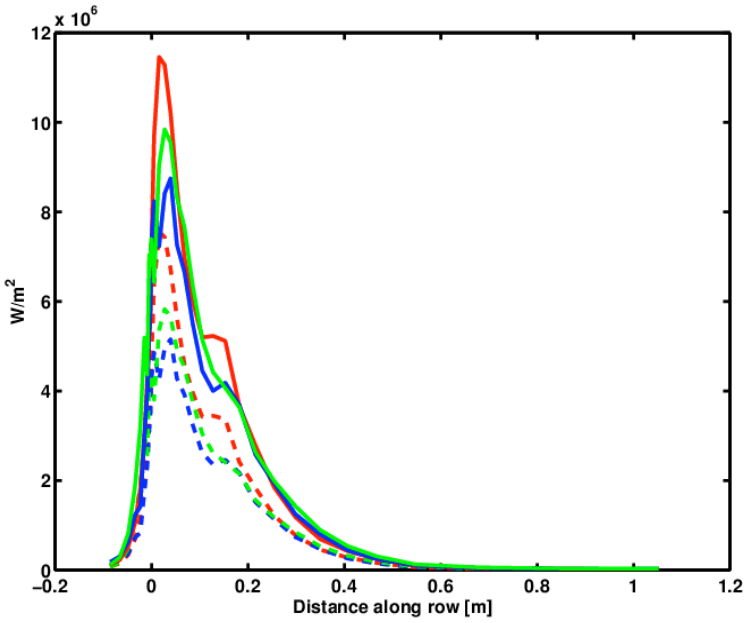

n_e

P_{out}

FIG. 11(b)

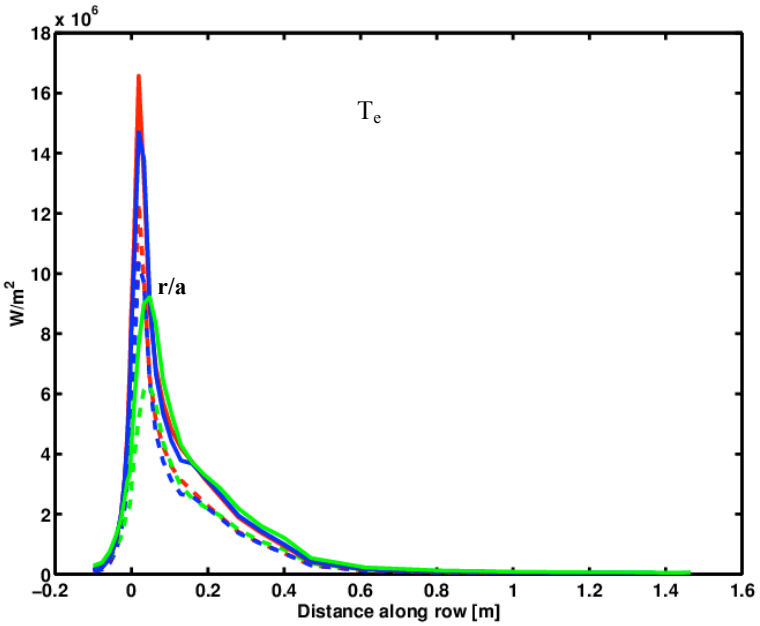

FIG. 12(a)

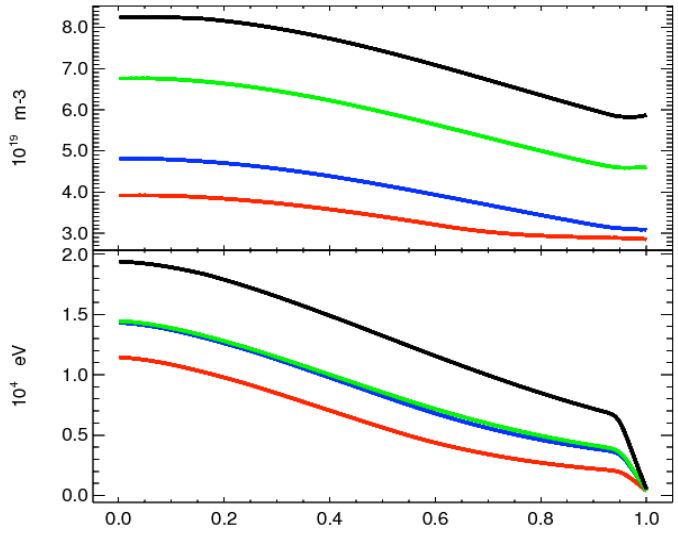

p

W_{th}[J]

T_i

Q

FIG. 12(b)

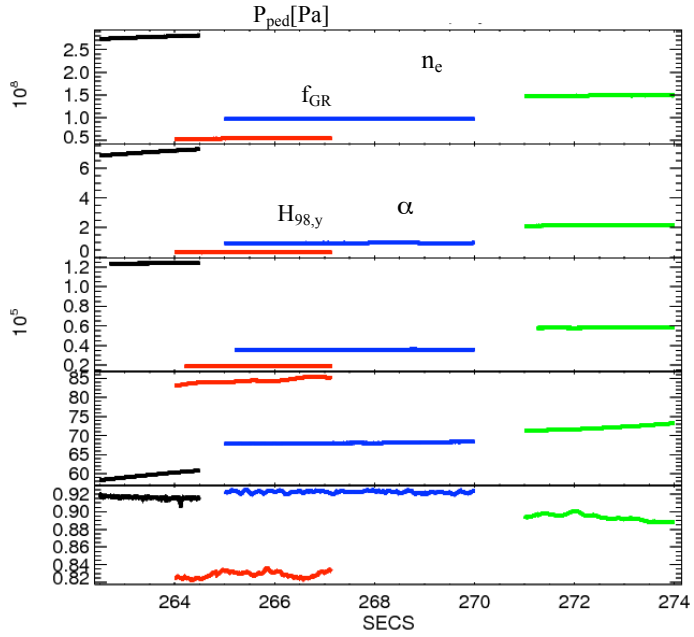

FIG. 13(a)

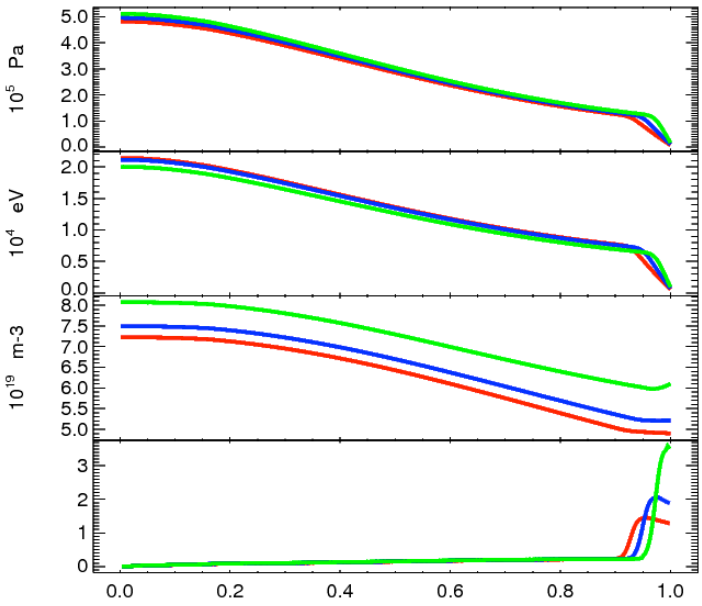

p

FIG. 13(b)

T_i

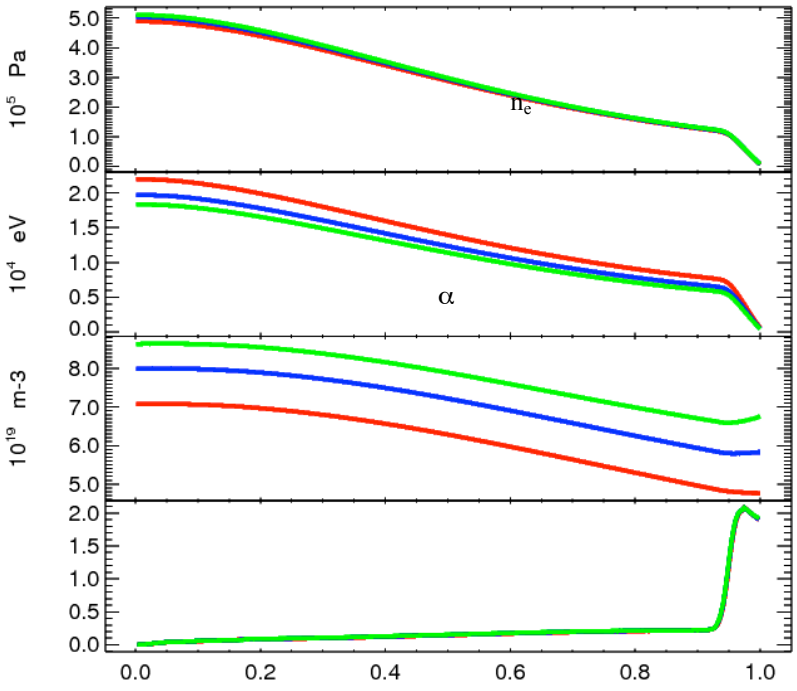
5.0
4.0
3.0
2.0
1.0
0.0
10^5 Pa
n_e
2.0
1.5
1.0
0.5
0.0
10^4 eV
α
8.0
7.0
6.0
5.0
10^19 m-3
2.0
1.5
1.0
0.5
0.0
0.0
0.2
0.4
0.6
0.8
1.0

TABLES

TABLE 1

	Scan 1			**Scan 2**		
	Case 1	Case 2	Case 3	Case 4	Case 5	Case 6
$\Gamma_{D,T}$ [10^{22}/s]	1.0	1.0	1.0	1.0	2.0	3.0
$\Delta_{ETB,etor,norm}$	0.09	0.07	0.05	0.07	0.07	0.07
$\Delta_{ETB\rightarrow SOL}$ [mm]	5-6	5-6	5-6	0	0	0
$\alpha_{crit,ETB}$	1.3	1.9	3.4	1.9	1.9	1.9
$n_{D+T,sep}$ [$10^{19}/m^3$]	4.9	5.2	6.0	4.7	5.8	6.7
$\Gamma_{D,T,neut,sep}$ [10^{21}/s]	2.0	1.8	1.4	1.4	2.4	0.5
$\chi_{e,sep}$ [m^2/s]	0.2	0.14	0.08	0.14	0.14	0.14
$T_{e,sep}$ [eV]	490	600	800	450	390	350
P_{SOL} [MW]	115	120	125	120	120	120
$\lambda_{q,out.midpl.}$ [mm]	~2.0	~1.5	~1.0	~6.0	~6.0	~5.5
max(q_{OT}) [MW/m^2]	19	23	19	14	12	9
W_{th} [MJ]	265	280	290	270	275	280
P_{fus} [MW]	375	400	415	385	400	-
$<n_e>$ [$10^{19}/m^3$]	5.9	6.3	-	5.8	6.8	-

CAPTIONS

FIG.1. *(a) Ψ map of the equilibrium for the 15MA case. (b) Vessel and target structure with dome, semi transparent surfaces and pump.*

FIG.2. *Details of divertor region grid used in the simulations*

FIG.3. *(a) From top to bottom, neutral source, electron density and temperature profiles vs normalised radius at 8s for 3 different levels of fuelling: 1.0 (magenta), 1.3 (red), $1.6x10^{22}$ s^{-1} (blue) for 15MA/5.3T ITER L-mode. Note how the central density is saturating at $2.9x10^{19}m^{-3}$ for higher puff rates. (b) From top to bottom, pinch velocity, diffusion coefficient, and electron heat conductivity profiles.*

FIG.4. *Radial profiles of the electron source in the SOL region near the separatrix at midplane for 3 different levels of fuelling: 1.0 (magenta), 1.3 (red), $1.6x10^{22}$ s^{-1} (blue) for 15MA/5.3T ITER L-mode. The distance along row is the distance from the separatrix (located at row 0.0) on a computational line perpendicular to the magnetic field (in the "radial" direction), see the EDGE2D grid in Fig.2.*

FIG.5. *Profiles of the ion temperature (top) and power flux (bottom) at the innner (left) and outer divertor (right) plates respectively for 3 different levels of fuelling: 1.0 (magenta), 1.3 (red), $1.6x10^{22}$ s^{-1} (blue) for 15MA/5.3T ITER L-mode. The distance along row is the distance from the separatrix (located at row 0.0) on a computational line parallel to the divertor plates in the "radial" direction, see the EDGE2D grid in FIG.2.*

FIG.6. *Time evolution of the volume averaged density (top) and temperature (bottom) for decreasing values of SOL diffusivities and constant puff rates. The radial profiles of the ion/electron thermal conductivities and the particle diffusivities are plotted in Fig.7. with same color code. The magenta trace has been obtained with SOL diffusivity 0.15 m^2s^{-1} and thermal conductivity 0.5* m^2s^{-1}

FIG.7. *Radial profiles of the electron (a) ion (b) conductivities and particle diffusivity (d) used in the simulations reported in Fig.6. The distance along row is the distance from the separatrix (located at row 0.0) on a computational line perpendicular to the magnetic field (in the "radial" direction), see the EDGE2D grid in Fig.2.*

FIG.8. *Time evolution of plasma parameters from L-mode into H =1 H-mode for a 15MA/5.3T plasma: (a) electron power to outer target (top), core neutral source inside the separatrix (bottom), (b) volume average core electron density (top) and separatrix ion temperature at divertor outer target (bottom).*

FIG.9. *Electron density (top) and temperature (bottom) in stationary H-mode, (a) $\Gamma_{DT} = 0.5\cdot10^{22}$ s^{-1} (red) and $1.0\cdot10^{22}$ s^{-1} (blue) at 5 MA / 5.3 T, (b) $\Gamma_{DT} = 0.5\cdot10^{22}$ s^{-1} (red), $1.0\cdot10^{22}$ s^{-1} (blue) $1.5\cdot10^{22}$ s^{-1} (green) and $2.0\cdot10^{22}$ s^{-1} (black) at 7.5 MA / 5.3 T (solid) and 7.5 MA / 2.65 T (dashed), (c) $\Gamma_{DT} = 0.75\cdot10^{22}$ s^{-1} (red), $1.25\cdot10^{22}$ s^{-1} (blue) and $2.0\cdot10^{22}$ s^{-1} (green) at 10 MA / 5.3 T.*

FIG.10. *(a) electron density (top) and temperature (bottom) profiles (b) from top to bottom: thermal energy, Q, D+T neutral influx at the separatrix, electron+ion heat flux at the separatrix, for a gas puff rate of $\Gamma_{DT} = 1.0\ 10^{22}$ s^{-1} (red), $2.0\ 10^{22}$ s^{-1} (blue) and $3.0\ 10^{22}$ s^{-1} (green) at 15 MA / 5.3 T.*

FIG.11. *Upper (solid) and lower (dashed) estimate for the power density on the inner (a) and outer (b) targets, for a gas puff rate of $\Gamma_{DT} = 1.0\ 10^{22}$ s^{-1} (red), $2.0\ 10^{22}$ s^{-1} (blue) and $3.0\ 10^{22}$ s^{-1} (green).*

FIG.12. (*a) electron density (top) and temperature (bottom) profiles (b), from top to bottom: time evolution of thermal energy, Q, pressure on top of the pedestal, fraction of Greenwald density limit and* $H_{98,y}$*, for the maximum DT gas puff rates that could be applied at 5 MA (red), 7.5 MA (blue), 10 MA (green) and 15 MA (black) without reaching detachment.*

FIG.13. *From top to bottom: profiles of thermal pressure, ion temperature, electron density, normalised pressure gradient. (a) Scan 1, Case 1 (red), 2 (blue) and 3 (green). (b) Scan 2, Case 4 (red), 5 (blue) and 6 (green) (cf. TABLE 1).*

TABLE 1. *Core and SOL plasma parameters for the simulation cases of two scans in ETB/SOL transport conditions mentioned in subsection 5.1. Values for the maximum local power density on the outer target plate max(*q_{OT}*) do not include power deposited by radiation and neutral interaction and are thus a lower-bound estimate.*